Use Authorization

In presenting this thesis in partial fulfillment of the requirements for an advanced degree at Idaho State University, I agree that the Library shall make it freely available for inspection. I further state that permission for extensive copying of my thesis for scholarly purposes may be granted by the Dean of the Graduate School, Dean of my academic division, or by the University Librarian. It is understood that any copying or publication of this thesis for financial gain shall not be allowed without my written permission.

Signature_____

Date_____

Identification of Volume of Distribution for Plutonium-239

by

Madeline Cook

A thesis

submitted in partial fulfillment

of the requirements for the degree of

Master of Science in the Department of Physics, Nuclear and Electrical Engineering

Fall 2019

To the Graduate Faculty:

The members of the committee appointed to examine the thesis of Madeline Cook find it satisfactory and recommend that it be accepted.

_____
Dr. Richard R. Brey,
Major Advisor

_____
Dr. Chad L. Pope,
Committee Member

_____
Dr. DeWayne R. Derryberry,
Graduate Faculty Representative

Acknowledgments

I would like to thank my parents Tom and Stephanie Cook for their endless love and encouragement. I would also like to thank Bryant and Leah Cook for all of their advice and support. A special thanks to my advisor Dr. Richard R. Brey for always believing in me and pushing me to do my best. Lastly I would like to express my appreciation to my committee members Dr. Chad L. Pope and Dr. DeWayne R. Derryberry for their invaluable feedback.

Table of Contents

List of Figures

List of Tables

Identification of Volume of Distribution for Plutonium-239

Thesis Abstract - Idaho State University (2019)

The work within identifies the volume of distribution (V_D) of plutonium using data from studies in which rats were administered an intravenous bolus injection of $^{239}Pu^{4+}$-citrate. The research investigated two separate datasets. Data published in Dr. P.W. Durbin's "Plutonium Deposition Kinetics in Rats" and studies conducted by Lovelace Respiratory Research Institute (LRRI) were examined. The goal of this research was to identify a value of V_D consistent with the known biological and physiological behavior of plutonium. The identified V_D is necessary to develop a physiologically based pharmacokinetic (PBPK) model. The creation of a PBPK model describing the behavior of plutonium in the body enables the comparison of transfer rates to validate the compartment models currently in use for internal dosimetry purposes. The V_D of a substance describes the distribution between intracellular and extracellular fluid compartments, providing information such as cellular uptake and protein binding. The V_D time profiles and values found using the Durbin data were consistent with known behavior of plutonium. The V_D values found using data provided by LRRI were not consistent with known behavior of plutonium, however the V_D time profiles generated may still be of use for PBPK modelling.

Key Words: volume of distribution, Pu-239, PBPK, compartment model, internal dosimetry

List of Abbreviations and Acronyms

BK	Biokinetic
BV	Blood volume
BW	Body weight
C_0	Instantaneous blood plasma concentration
C_P	Plasma concentration
ECF	Extracellular fluid
F344	Fischer 344
hTF	Human serum transferrin
ICF	Intracellular fluid
ICRP	International Commission on Radiological Protection
INL	Idaho National Laboratory
IV	Intravenous
LLRI	Lovelace Respiratory Research Institute
NIST	National Institute of Standards and Technology
PBPK	Physiologically based pharmacokinetic
Pu	Plutonium
RBCs	Red blood cells
S-D	Sprague-Dawley
Tf	Transferrin
TFRs	Transferrin receptors
V_D	Volume of distribution
V_C	Instantaneous volume of distribution

V_{SS}	Volume of distribution at steady-state
$V_{area/\beta}$	Volume of distribution at terminal elimination phase

Chapter 1: Introduction

The science of internal dosimetry assesses the dose from ionizing radiation that will be delivered by radioactive materials that have entered the body through the primary exposure pathways: inhalation, ingestion, transdermal absorption, and wound contamination. The internal hazard must be characterized in the event of an occupational, medical, or environmental exposure to radioactive material. The methodology of dose assessment involves the use and development of biokinetic (BK) models to describe the deposition, retention, and elimination of specific radionuclides from within the body. The behavior of radionuclides detailed by BK models is necessary for predicting initial intake, internal dose assignment, and organ-level absorbed doses. This information aids the determination of risk associated with the intake and supports medical intervention decision-making.

1.1 Problem Statement

The International Commission on Radiological Protection (ICRP) has recommended a series of ever more sophisticated biokinetic models built using available human case and animal experimental data including the publication 67 plutonium (Pu) systemic model. Due to its use in nuclear energy and the production of nuclear weapons, there is potential for occupational and public exposure to Pu. Consequently there is a need for internal dose assessment optimization to adequately respond in the event of a Pu intake. Although the BK models recommended by the ICRP contain physiologically based compartments representative of organs and tissues, the transfer rates between these compartments are primarily calculated using computational and mathematical methods. Estimates of transfer rates based on direct physiological kinetics could

support those values obtained by mathematically fitting excretion data and post mortem concentrations.

The pharmaceutical industry has examined a comparable method for modeling the absorption, distribution, metabolism, and excretion (ADME) of drugs within the body known as physiologically based pharmacokinetic (PBPK) modeling. This modeling approach integrates physiological variables and compound specific properties to characterize drug activity. The development of a PBPK model in which Pu is treated as the "drug" for which ADME is being described, may corroborate compartment modeling methods recommended by the ICRP. A comparison between these methodologies to validate the transfer coefficients of the Pu systemic model currently in use if indeed possible, is desirable. There exists a need for the identification of the key parameter, volume of distribution (V_D), for the development of a Pu PBPK model. Data from $^{239}Pu^{4+}$-citrate intravenous (IV) bolus injection rat studies are used to determine the volume of distribution for Pu.

1.2 Research Objectives

The purpose of this research is to identify the volume of distribution for plutonium-239. The volume of distribution of a material is the theoretical volume of body fluid required for the total amount of administered material in the body to reach the measured plasma or blood concentration. A large volume of distribution indicates the substance has been widely dispersed throughout the body, occupying intracellular fluid (ICF) space. A small volume of distribution suggests the substance has primarily remained within the extracellular fluids (ECF). The volume of distribution as a function of time compared to the ECF and ICF volumes provides information such as protein-binding, cellular uptake, and lipophilicity. This value and its associated characteristics will be used as a basis for developing transfer rate coefficients for translocation

among physiological compartments. These transfer coefficients will be compared to the values obtained by the system of compartmental models developed using the methods of ICRP.

Volume of distribution is represented by the following equation:

$$V_D\ (mL) = \frac{amount\ of\ administered\ dose\ in\ the\ body\ (\%)}{plasma\ concentration\ (\%/mL)} \quad (1.1)$$

Knowledge of Pu suggests V_D shall initially be less than or equal to the blood plasma volume due to transferrin (Tf) protein binding. To be consistent with anticipated behavior of Pu and other bone-seeking radionuclides, the V_D should rapidly increase to exceed the volume of the ECF compartment. This is indicative of the assumed cellular uptake and retention of Pu, primarily in bone and liver tissues.

1.3 Hypothesis Testing

The following hypotheses will be tested in this research:

$H_{1,0}$: The volume of distribution identified using data presented in Table 3 of Patricia Durbin's "Plutonium Deposition Kinetics in Rats" is consistent with known behavior of plutonium.

$H_{1,A}$: The volume of distribution identified using data presented in Table 3 of Patricia Durbin's "Plutonium Deposition Kinetics in Rats" is not consistent with known behavior of plutonium.

The null hypothesis will be consistent if the volume of distribution identified using the Durbin data set is less than or equal to ECF volume at time t = 0, and greater than ECF volume within 24 hours of intake. In the event the volume of distribution is found to be greater than ECF volume at time t = 0 and/or less than ECF volume after 24 hours following intake, the null hypothesis will be rejected in favor of the alternate hypothesis.

$H_{2,0}$: The volume of distribution identified using data from studies conducted by Lovelace Respiratory Institute is consistent with known behavior of plutonium.

$H_{2,A}$: The volume of distribution identified using data from studies conducted by Lovelace Respiratory Institute is not consistent with known behavior of plutonium.

The null hypothesis will be consistent if the volume of distribution identified using the Lovelace data set is less than or equal to ECF volume at time t = 0, and greater ECF volume within 24 hours of intake. In the event the volume of distribution is found to be greater than ECF volume at time t = 0 and/or less than ECF volume after 24 hours following intake, the null hypothesis will be rejected in favor of the alternate hypothesis.

Chapter 2: Literature Review

2.1 Characteristics of Plutonium

Since the commencement of the Manhattan Project there has been a significant need for the greater understanding of the effects of radioactive materials on living organisms. This research engendered an interest in the fissionable radioisotope plutonium-239 due to its presence in nuclear fuel and weapons production. In-depth studies on the behavior and characteristics of this material have been essential to human health in the event of an intake. Recent events include a plutonium spill at the National Institute of Standards and Technology (NIST) Boulder laboratory, exposing several personnel in 2008. Accidental exposures have also occurred at the Idaho National Laboratory (INL) in recent years, including an airborne release of Pu in 2011 followed by a transuranic wound contamination in 2018. Although implementation of safety procedures should aid in the prevention of such events, an understanding of the physical, chemical, and biological characteristics of Pu is imperitive to proper response.

2.1.1 Physical and Chemical Properties of Plutonium

Plutonium is the sixth member of the actinide series in the periodic table, denoted by the chemical symbol Pu and atomic number 94. This transuranic element is a silvery metal of varying allotropes with densities between 15.92 to 19.86 g/cm^3 (Miner 1964). Although plutonium is a metal, several of its characteristics set it apart from this group of elements. For example Pu has a relatively low melting point of 640 °C, however its boiling point remains high at 3,227 °C (Miner 1964). Also, contrary to most metals, the thermal and electrical conductivity of Pu is very low (Miner 1964).

The characteristic 5f valence electrons of the actinide metals enable this group of elements to bond more readily than their lanthanide neighbors (Clark 2000). Plutonium is able to form compounds with most metals and halogens as well as react with hydrogen and oxygen (LANL 2013). Pu has five oxidation states with the possibility of up to four existing at once in specific chemical environments: Pu(III), Pu (IV), Pu(V), Pu(VI), and Pu(VII) (Clark 2000). The oxidation state largely dictates the chemical behavior of plutonium.

There are currently 23 identified isotopes of plutonium with mass numbers 228 to 247 (LANL 2013). According to the U.S. Nuclear Regulatory Commission (NRC), there are five common isotopes of plutonium, all of which are fissionable and decay through alpha emission (NRC 2017).

Table 2.1: Properties of the five most common plutonium isotopes

Isotope	Half-life (y)	Decay mode
Pu-238	87.74	α
Pu-239	2.41×10^{4}	α
Pu-240	6.56×10^{3}	α
Pu-241	14.35	α, β
Pu-242	3.73×10^{5}	α

Although Pu is primarily considered an anthropogenic element, it does exist in small quantities in nature. The trace amount of Pu-244 in nature is attributed to the isotope's 80 million year half-life (Miner 1964). Pu-238 and Pu-239 are found in sparse quantities concentrated in uranium ore due to natural nuclear reactions (Miner 1964). The formation of Pu-238 is the result of a double beta decay of U-238 (LANL 2013). Pu-239 is naturally created via neutron capture of uranium-238 (Miner 1964).

Plutonium-238 and Pu-239 appear to be the most important isotopes of Pu when examining occupational and public exposures. This is due to their presence in electric power generation and military applications. Pu-238 was first produced via the bombardment of U-238

with deuterons to result in neptunium-238 and two neutrons (Seaborg 1946). Np-238 has a half life of approximately 2 days and decays via isobaric negatron emission to produce Pu-238 (Seaborg 1946).

$$^{238}_{92}U\ (d,2n)\ ^{238}_{93}Np \xrightarrow{\beta^-} ^{238}_{94}Pu \tag{2.1}$$

High purity Pu-238 can also be produced by irradiating an americium-241 or neptunium-237 target with high energy neutrons (Jones 2002). Pu-238 is primarily used as an energy source for power generation during space missions (Oakley 2017).

$$^{237}_{93}Np(n,\gamma)\ ^{238}_{93}Np \xrightarrow{\beta^-} ^{238}_{94}Pu \tag{2.2}$$

Plutonium-239 is produced in a nuclear reactor when U-238 absorbs a neutron to form U-239. U-239 undergoes isobaric transition to become Np-238 which also undergoes beta decay to result in Pu-239.

$$^{238}_{92}U(n,\gamma)^{239}_{92}U \xrightarrow{\beta^-} ^{239}_{92}Np \xrightarrow{\beta^-} ^{239}_{94}Pu \tag{2.3}$$

Pu-239 is the most common isotope due to its formation in reactors, ability to be reprocessed as fuel, and fissionability desirable for atomic weapons.

2.1.2 Biological Behavior of Plutonium

As previously discussed plutonium exists in up to four different oxidation states (III-VI) at one time under environmental conditions. However, Pu(IV) is the most important when examining biological behavior due to its stability within cells (Aryal et al. 2011). At physiological pH, Pu(IV) is hydrolyzed to form polymeric plutonium (Aryal et al. 2011). In the event of an intake of highly polymeric Pu, retention in liver and skeletal tissue is largely due to phagocytosis (Weber et al. 2014). Monomeric plutonium behaves differently than polymeric solutions. Deposition of monomeric Pu is approximately equal between liver and bone (Schubert

et al. 1961). Polymeric Pu is colloidal in nature and is retained in the liver and spleen at higher rates with less bone retention than monomeric form (Schubert et al. 1961).

The radius ratios of Pu^{4+} and Fe^{3+} are similar, causing them to have similar biological behaviors (Jensen et al. 2012). The resemblance between iron (Fe) and plutonium at physiological conditions has led to many assumptions about the biological behavior of Pu. In order to better understand this relationship, the role of Fe in the body should be discussed.

Iron is a central component for many important cell functions including oxygen delivery, electron transport for metabolic processes, or as a cofactor or enzyme component in many cellular reactions (Gupta 2014). Fe is an essential nutrient vital to many of the oxidation-reduction reactions that take place in the body (Insel et al. 2011). This property is due to the ferrous and ferric oxidation states of iron (Insel et al. 2011). Ferrous iron (Fe^{2+}) can be oxidized to ferric iron (Fe^{3+}), which can in turn be reduced back to the ferrous state (Whitney et al. 2011). Fe levels are highly regulated due to its essential role in maintaining cell function as well as it's toxic effects at high concentrations (Whitney et al. 2011). Although approximately 70% of the body's Fe is contained in red blood cells (RBCs), proteins such as ferritin and transferrin bind the ion and store or deliver it where needed (Gupta 2014). Less than 0.1% of the body's iron is anticipated to be attached to Tf at any instant in time (Kohgo et al. 2008).

When iron is plentiful, the excess stored in ferritin located in the small intestine will be shed along with mucosal cells and excreted (Smolin et al. 2010). When iron is needed, it is transferred to Tf (Smolin et al. 2010). Transferrin also binds iron to be recycled from degraded RBCs in the liver (Whitney et al. 2011). In order for Tf to bind iron, it must be in the ferric state (Smolin et al. 2010). Due to the acidic conditions of the intestine, iron is in its reduced ferrous form (Abbaspour et al. 2014). During transportation across mucosal cells to the blood, ferrous

iron is oxidized to ferric iron by integral membrane proteins (Smolin et al. 2010) (Fig 2.1). At physiological pH, the iron will remain in ferric form (Abbaspour et al. 2014).

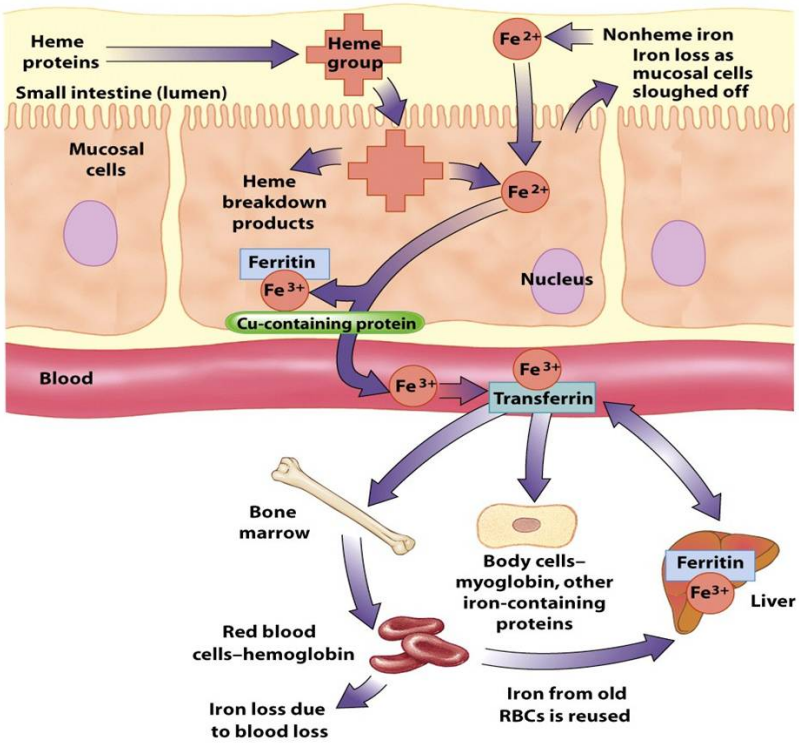

Fig 2.1. Absorption of dietary iron (Smolin et al. 2010).

Human serum transferrin (hTF) is a transferrin protein synthesized in the liver and secreted into blood plasma (Wally et al. 2006). It is a bilobal protein with the ability to bind up to two iron ions, one in each lobe (Steere et al. 2012). The lobes of hTF are formed by four subdomains in which N1 and N2 domains comprise the N-lobe and C1 and C2 subdomains comprise the C-lobe (Wally et al. 2006) (Fig. 2.2). Given the structure of hTF, there are several different states in which it exists in the body depending on iron levels (Steere et al. 2012). These states are diferric in which both lobes contain ferric iron, monoferric N-lobe, monoferric C-lobe, and iron-free hTF (Steere et al. 2012).

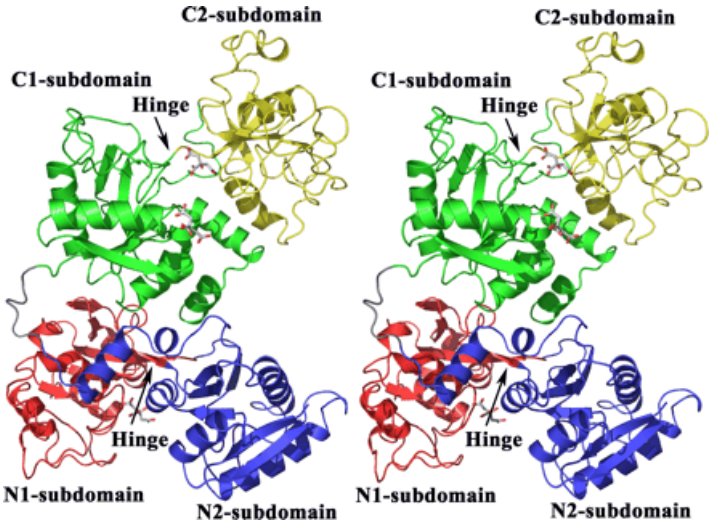

Fig. 2.2. Transferrin subdomains (Wally et al. 2006).

In both the N- and C-lobes, ferric iron is held in place by the ligands of the two subdomains (Steere et al. 2012). The N1 and C1 subdomains are comprised of one aspartic acid (Wally et al. 2006). The hinge bordering the N1 and C1 subdomains contain a histidine residue (Wally et al. 2006). Two tyrosines are located within and at the hinge of the N2 and C2 subdomains (Wally et al. 2006). As seen in Figure 2.3, an arginine anchored carbonate is also involved (Steere et al. 2012).

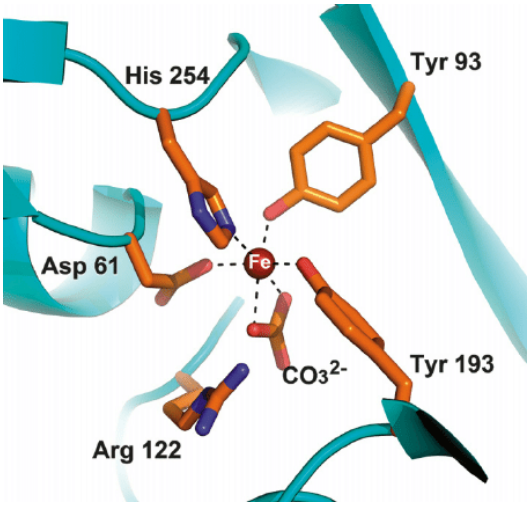

Fig. 2.3. Transferrin ligands binding ferric iron (Baker 2012).

Transferrin delivers iron to the cells by binding to and forming a complex with transmembrane glycoproteins called transferrin receptors (TFRs) (Turgeon 2012). All cells that require iron to carry out cellular processes contain TFRs on their membrane surfaces (Steere et al. 2012). The complex then enters the cell via endocytosis as shown in Figure 2.4 (Steere et al. 2012). The pH change from 7.4 in the blood to 5.6 within the endosome causes transferrin to release the iron (Steere et al. 2012). This drop in pH is due to integral proteins that act as ATP-driven proton pumps (Steere et al. 2012).

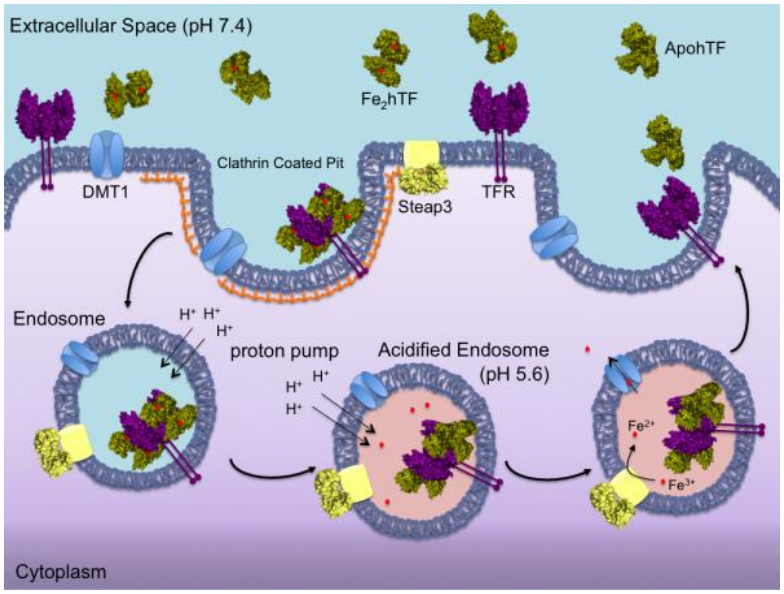

Fig. 2.4. Endocytosis of tf-tf receptor complex (Steere et al. 2012).

Once released from transferrin, ferric iron is converted to ferrous iron via ferrireductase enzyme incorporated in the endosomal membrane (Steere et al. 2012). The Fe^{2+} ion is then passed through the divalent metal transporter channel to the cytosol of the cell (Steere et al. 2012) (Fig. 2.4). The endosome then recombines with the cell membrane to release the transferrin-transferrin receptor complex where the iron delivery cycle can continue (Steere et al. 2012).

Due to the Pu^{4+} valence state showing similar biological behavior to that of Fe^{3+} in the body, the relationship between Pu and Tf has been closely studied. Using several techniques including receptor binding assays, x-ray scattering and fluorescence microscopy, transferrin has been shown to bind to plutonium (Jensen et al. 2011). Given the four previously described states of hTF, the addition of plutonium to the system introduces several new possible transferrin complexes.

One possible conformation includes two Pu ions, one in each of the N- and C-lobes. A plutonium in the N-lobe with an iron in the C-lobe, and vice versa are also possibilities considered (Jensen et al. 2011). The final conformation thought to be possible is Pu in just the N- or C- lobe with the other not bound to any ions (Jensen et al. 2011). It was found that only one of the possible conformations was able to enter the cells (Jensen et al. 2011). This is because when transferrin binds ions, the structure slightly changes so it is better recognized by transferrin receptors. The active form of the plutonium-transferrin complex capable of entering cells consists of Fe^{3+} bound to the protein's N-lobe and Pu^{4+} within the C-lobe as it more closely resembles the structure and shape of diferric transferrin (Jensen et al. 2011) (Fig. 2.5).

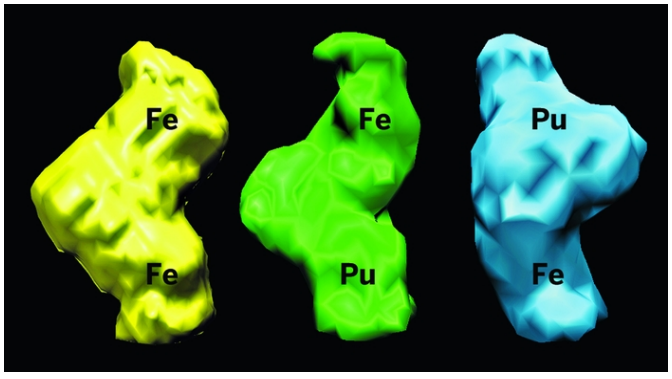

Fig. 2.5. Diferric transferrin (yellow), Fe^{3+} in N-lobe with Pu^{4+} in C-lobe (green), Fe^{3+} in C-lobe with Pu^{4+} in N-lobe (blue) (Jensen et al. 2011).

Upon entering a cell, Pu may then associate with the iron storage protein ferritin in tissues such as liver, spleen, and bone marrow (Taylor 1973). Although Pu readily forms stable

bonds with the proteins Tf and ferritin, its behvaior regarding RBC incorpotation has not been concluded. It is believed Tf provides a pathway for Pu incorporation into RBCs. As previously mentioned, most of the body's Fe is located in RBCs. Similarly to Fe, Tf delivers Pu to bone marrow where erythropoiesis takes place. Although Pu cannot be incorporated into mature RBCs, it may be incorporated into those which are in the stages of development at the time of intake (Moss, Eckhardt 1995). Several days after Pu incorporation, approximately 10% of the developing RBCs are catabolized (Moss, Eckhardt 1995). This event may describe the turnover of activity from bone marrow back to blood (Fig 2.6). Another opinion states that despite delivery of Pu to bone marrow, it has been found that Pu does not associate with the hemoglobin or stroma of RBCs (Durbin 2008). The failure of erythroblasts, immature RBCs, to endocytize Pu is thought to be to due the inability of erythroblast TFRs to recognize the Tf-Pu complex (Durbin 2008).

The risk of Pu exposure has engendered interest in counter preventative measures in the case of a worker or public intake. Chelation therapies are employed to sequester and eliminate plutonium when necessary. The biological behavior of Pu in the body must be well-known to estimate and optimize the efficacy of these therapies as well as aid the determination of the initial intake and associated risk to human health.

2.2 ICRP 67 Plutonium Systemic Model

The ICRP publication 67 (ICRP 1993) recommended biokinetic model is the current method for assessing dose from plutonium intake (Fig 2.6). The compartments of the model are physiologically based representations of affected organs and tissues with one central blood compartment assumed to be a uniformly mixed pool (ICRP 1993). Pu is translocated between the

blood compartment and three soft tissue compartments, each representing rapid, intermediate, and slow turnover rates. The rapid exchange compartment is denoted by ST0 and returns activity to the blood within hours to days. The intermediate turnover soft tissue compartment, ST1, returns Pu to the blood within two years. Retention occurs for several years in the soft tissues with slow turnover. During this retention period Pu may exist in protein bound ionic form or insoluble particulate form (Taylor 1973). Activity in the ST1 compartment may be returned to the blood or delivered to the urinary bladder contents compartment for excretion.

In addition to the urinary path compartments, the kidneys include a compartment for other kidney tissues. The other kidney tissues compartment demonstrates recycling with the blood. By contrast, plutonium is eliminated once introduced to the urinary path and urinary bladder contents compartments. Another route of elimination in the ICRP 67 model includes fecal excretion via GI tract contents compartment which collects activity from the blood and liver. Pu is transferred from the blood to the upper large intestine (ULI) of the GI tract contents while the small intestine absorbs activity from liver 1. The liver is divided into two compartments with liver 1 receiving Pu from the blood which may then be translocated to blood, liver 2, or the GI tract. Liver 2 obtains activity from the liver 1 compartment and may recycle back to the blood. Plutonium is also exchanged between the blood and skeletal tissue.

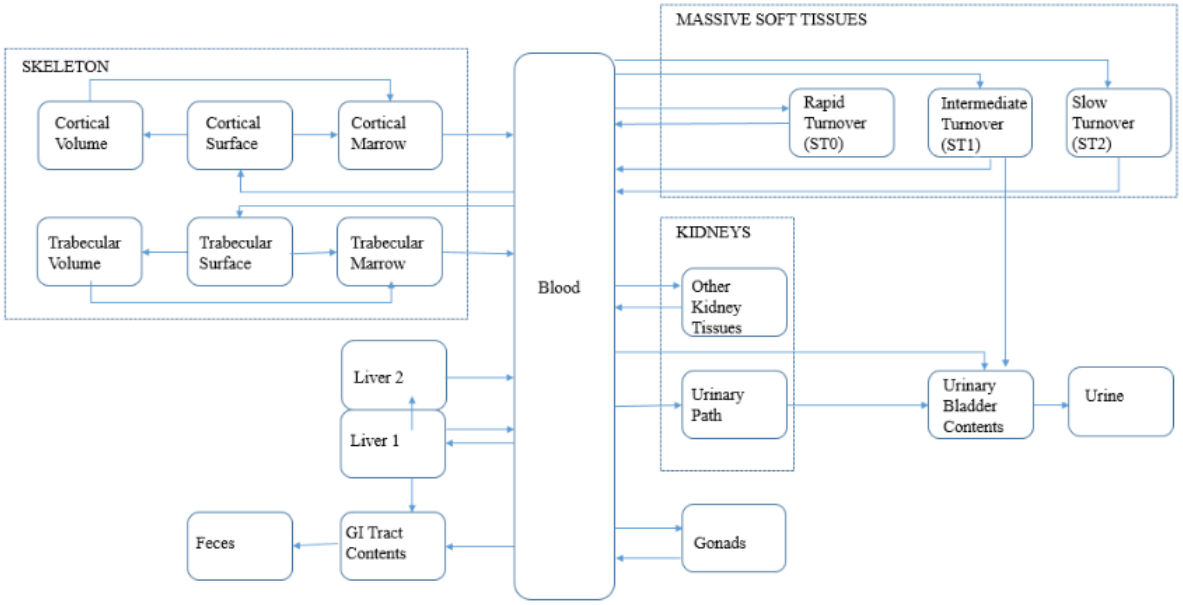

Fig. 2.6. Diagram of the ICRP publication 67 plutonium systemic model (ICRP 1993)

The skeletal compartments constitute the two types of bone tissues, cortical and trabecular, and are further broken down to depict the movement from the volume, surface, and marrow structures of each. Activity is transferred from the blood to the surface compartments of trabecular and cortical bone. Each surface has two pathways in which activity is lost, delivery to the volume and marrow compartments of the respective skeletal tissues. Pu may be translocated from the cortical and trabecular volume compartments to respective marrow tissues where some activity is returned to the blood.

Table 2.2: ICRP 67 transfer rates for plutonium biokinetic models

Route	Transfer Rate (day^{-1})
ST0 to Blood	6.93E-01
ST1 to Blood	4.75E-04
ST2 to Blood	1.90E-05
Trabecular marrow to Blood	7.60E-03
Cortical marrow to Blood	7.60E-03
Kidneys (other tissue) to Blood	1.39E-03
Liver2 to Blood	2.11E-04
Testes to Blood	1.90E-04
Ovaries to Blood	1.90E-04
Blood to ST0	2.773E-01
Blood to ST1	8.06E-02
Blood to ST2	1.29E-02
Blood to Trabecular surface	1.941E-01
Blood to Cortical surface	1.294E-01
Trabecular surface to Trabecular volume	2.47E-04
Cortical surface to Cortical volume	4.11E-05
Trabecular surface to Trabecular marrow	4.93E-04
Trabecular volume to Trabecular marrow	4.93E-04
Cortical surface to Cortical marrow	8.21E-05
Cortical volume to Cortical marrow	8.21E-05
Blood to Kidneys (other tissue)	3.23E-03
Blood to Liver1	1.941E-01
Liver1 to Liver2	1.77E-03
Blood to Testes	2.30E-04
Blood to Ovaries	7.10E-05
Liver1 to Small intestine	1.33E-04
Blood to Upper large intestine	1.29E-02
Blood to Kidneys (urinary path)	6.47E-03
Blood to Bladder	1.29E-02
ST1 to Bladder	4.75E-04
Kidneys (urinary path) to Bladder	1.386E-02

The compartment model published in ICRP 67 is the most current iteration describing the biokinetics of plutonium. It is used for calculating dose coefficients for occupational intakes as recommended in ICRP 68 (ICRP 1994). ICRP 67 is also the basis for interpreting in vivo and in vitro bioassay measurements proposed in ICRP 78 (Konzen et al. 2015).

2.3 PBPK Models

Physiologically based pharmacokinetic (PBPK) modelling is another approach to describing the biological behavior of a substance. It is used in the pharmaceutical industry for the

development of drugs by predicting their absorption, distribution, metabolism, and elimination (ADME). PBPK models incorporate physicochemical properties of the drug, and organism specific physiology and anatomy (Kuepfer et al. 2016). Compound specific characteristics implemented in PBPK include lipophilicity, molecular weight, and solubility. Physiological parameters include blood flow rates, organ volumes, and tissue surface areas (Kuepfer et al. 2016). Mode of administration is also taken into consideration in PBPK modelling.

Two key parameters for building a PBPK model are clearance and volume of distribution. Clearance (CL) is defined as the volume of plasma from which the drug has cleared over a period of time (Jones 2013). Total clearance is the summation of clearance via fecal and urine excretion as well as the metabolism of the drug (Jones 2013).

$$CL_{total} = CL_{hepatic} + CL_{renal} + CL_{other} \quad (2.4)$$

In the case of plutonium it is assumed Pu is not further metabolized and therefore only clearance via urine excretion or biliary pathway excretion to the gut is necessary for determining this parameter.

Volume of distribution (V_D) is the volume of body fluid the drug must be distributed within in order to obtain measured plasma or blood concentrations (Davis et al. 2011). V_D is often referred to as a "theoretical volume" because it does not represent a singular physiological space, rather it describes the distribution of a drug relative to the body's three basic fluid volume compartments (Fig. 2.7.).

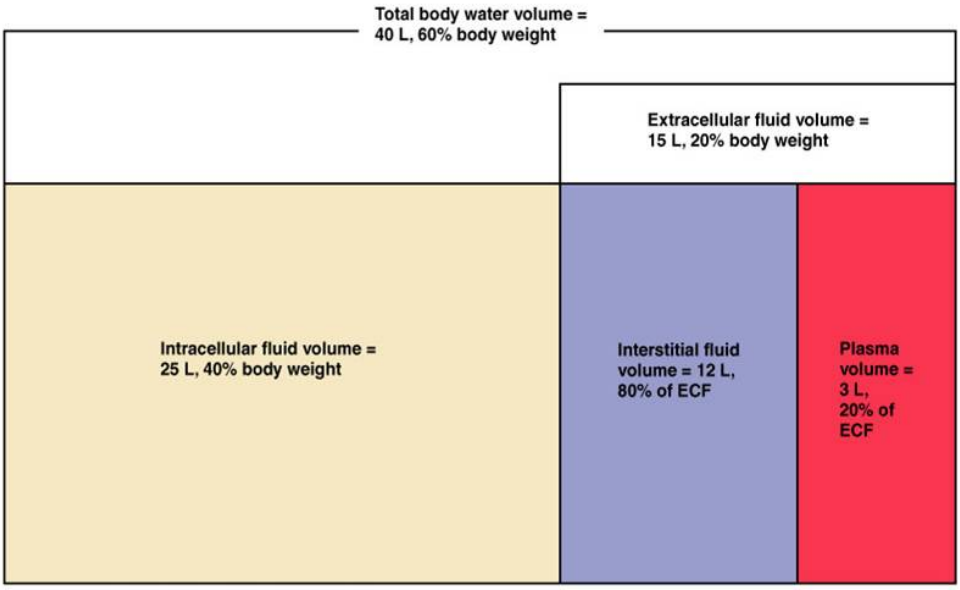

Fig. 2.7. Adult human body fluid compartment volumes

A volume of distribution exceeding the volume of extracellular fluid, 15 L in the case shown in Fig 2.7, suggests the drug has undergone cellular uptake and no longer remains exclusively in the blood or interstitial spaces. Conversely a small V_D (less than 3 L in this example) implies the drug is bound to a blood protein or unbound in the blood plasma and has not permeated organ tissues. Both CL and V_D are time dependent and are used to calculate the effective half-life of a drug (Jones 2013).

Similar to the BK modeling recommended by the ICRP, PBPK models only include organs and tissues pertinent to the drug being examined. A major difference however is the treatment of blood. While ICRP BK models treat blood as a singular central compartment assumed to be a uniformly mixed pool, PBPK models express systemic circulation with two separate blood compartments (Fig. 2.8). One compartment represents oxygenated arterial blood which is delivered to the cells of organs and tissues while the second compartment demonstrates the return of deoxygenated venous blood. Moreover, compartment models rarely take into

consideration the dynamics of the suspension of components that are grouped into the concept called blood.

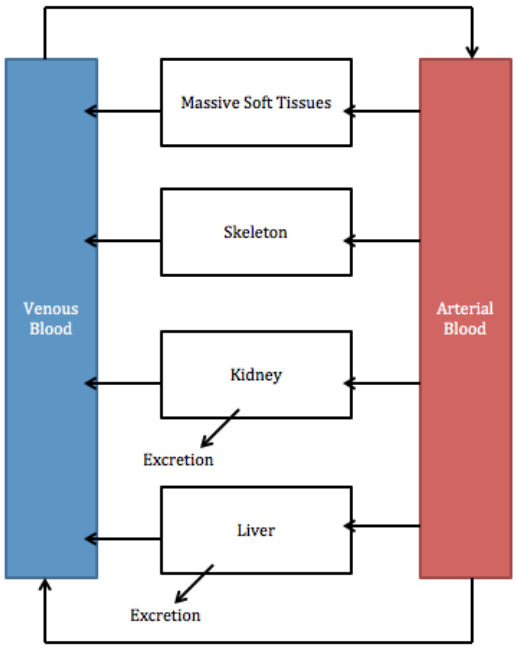

Fig. 2.8. Reduced PBPK model comparable to ICRP 67 plutonium biokinetic model.

Although there are nuances in format, these methods are comparable as they both model biological behavior. For example, the delivery rate from arterial blood to the kidney tissues in PBPK is comparable to the transfer rate between the blood and kidney tissues in ICRP 67. The return of activity from the kidney tissue compartment to the central blood compartment described in ICRP 67 is instead denoted as transfer to the venous blood in a PBPK model. This similarity enables the validation of transfer coefficients to support the predictability of ICRP 67 compartment models.

Chapter 3: Materials and Methods

3.1 Overview of data

In this work two sets of data are examined, each involving the administration of $^{239}Pu^{4+}$-citrate to rats via bolus IV injection. Data published in Dr. P.W. Durbin's "Plutonium Deposition Kinetics in Rats" describe the deposition of Pu within 48 hours of administration. The data provided in this publication is a compilation from various experiments using young adult female Sprague-Dawley (S-D) rats (Table 3.1). The data of Schubert *et al.* is referred to as the "basic data" in the publication as it is used as the primary source for tissue distribution in S-D rats (Durbin 1972). Excreted activity and bound versus unbound blood plasma content were not measured in the basic data. To compensate for this, these values were calculated using data from studies with similar experimental conditions (Durbin 1972).

Table 3.1: Distribution of Pu in rat tissues* used to calculate V_D (Durbin 1972)

Time (hr)	Total plasma (% of dose)	Excreta** (% of dose)	Plasma (%/mL)
0.125	52.5	0.1	6.5
0.25	45.6	0.9	5.6
0.5	41.5	1.4	5.1
1	38.0	2.1	4.7
2	33.9	2.8	4.2
6	27.1	4.1	3.3
12	17.4	5.2	2.2
24	6.1	5.8	0.75
48	1.8	-	0.22

*Schubert et al.

** Calculated from data of Carritt et al.

Data provided by LRRI detail the distribution of Pu in rats after bolus IV injection through a jugular vein cannula (see Appendix A for the complete data set used in the calculation of V_D). The subjects used in this study were Fischer 344 (F344) rats 9 to 13 weeks of age. A total of 48 rats were used in this study with eight groups of six rats, three male and three female. The

groups were based on different times of sacrifice: 1 hour, 4 hours, 24 hours, 2 days, 4 days, 8 days, 16 days, and 28 days after administration (Table 3.2).

Table 3.2: Dose given to experimental groups of differing sacrifice times (LLRI, 2009)

Animal Group	Dose Administration	Necropsy
F1-F6	Pu-239 (200nCi, 0.2 mL)	1 hr
E1-E6	Pu-239 (200nCi, 0.2 mL)	4 hr
D1-D6	Pu-239 (200nCi, 0.2 mL)	24 hr
G1-G6	Pu-239 (200nCi, 0.2 mL)	2 d
C1-C6	Pu-239 (200nCi, 0.2 mL)	4 d
H1-H6	Pu-239 (200nCi, 0.2 mL)	8 d
B1-B6	Pu-239 (200nCi, 0.2 mL)	16 d
A1-A6	Pu-239 (200nCi, 0.2 mL)	28 d

The rats were received one week prior to the day of dosing to allow for acclimation and quarantine in metabolism cages. Subjects were kept in metabolism cages for the entirety of the study to allow for daily collection of urine and feces. They were randomized at least one day before administration of Pu. The Pu administered in this experiment was Pu-239 formulated as a citrate with pH 6.0 resulting in an activity of 1.0 μCi/mL. Rats were injected with 0.2 mL of $^{239}Pu^{4+}$-citrate for a total activity of 200 nCi per animal (Table 3.2).

3.2 Calculation of Volume of Distribution

To test the hypotheses, V_D was calculated at times t = 0 and 24 hours using the data in several ways. The first approach uses the time, excreta, and plasma concentration (C_P) values published in Durbin's "Plutonium Deposition Kinetics in Rats" (Table 3.1). V_D at time t = 0 is commonly referred to as volume of distribution of the central compartment (V_C). After IV injection, the compound instantaneously distributes in blood plasma as the central compartment (Schrag & Regal, 2013).

The decrease in plasma concentration after IV injection is typically described by a monoexponential or multiexponential equation representative of monophasic or multiphasic distribution (Schrag & Regal, 2013). The instantaneous blood plasma concentration (C_0) was

calculated by plotting C_P versus time and fitting the data with a best-fit exponential curve. C_0 was then extrapolated by solving the double-exponential equation for x = 0. V_C was then calculated using equation 1.1 where it is assumed 100% of the dose is present in the body instantaneously after injection:

$$V_C(mL) = \frac{Total\ administered\ dose}{C_0} \quad (3.1)$$

V_D for t = 24 hours was calculated by subtracting the percent activity lost in urine and fecal excretion within 24 hours of the dose and dividing it by the recorded blood plasma concentration value for 24 hours.

The LRRI data did not include plasma concentration. Instead the percent of dose recovered from blood at the time of sacrifice was measured. To find C_P the total blood volume must be known. Blood volume (BV) was calculated using the approximate body weight (BW) of male and female rats used in the study (Lee & Blaufox 1985).

$$BV\ (mL) = 0.06*BW(kg)+0.77 \quad (3.2)$$

The percent of recovered dose in the blood divided by blood volume is used as the C_P for calculating V_D for the LRRI data. The calculations performed with the Durbin data were repeated using LRRI data to examine the V_D in several ways. V_D was calculated for individual rats, the average of all six rats in a necropsy group, only females of the group, and only males of the group.

3.3 Interpreting Volume of Distribution

As previously stated, V_D is not an actual anatomical volume within the body but rather a theoretical space used to describe the distribution of Pu. To understand the information provided by the calculated V_D, the body fluid compartment volumes for the rats must be determined. As shown in Figure 2.7, two primary compartments of fluid can be compared to V_D: extracellular

and ICF volumes. The ECF volume is further broken down to represent plasma volume and interstitial fluid volume.

It is assumed material occupying the intracellular volume (ICF) has undergone cellular uptake. Material within the plasma volume of the ECF exists in one of two states: bound or unbound to proteins. Pu is unlikely to exist in ionic form in blood as it readily forms complexes, primarily with Tf (Priest 1990). Due to this behavior, the majority of activity in this compartment is protein bound. It has been found that within one week of IV administration 95% of Pu in this fluid compartment is protein bound (Durbin 1972). The interstitial fluid volume is the area between blood vessels and cells (Fig. 3.1). In this space, exchange of nutrients or wastes occurs between the blood and cells.

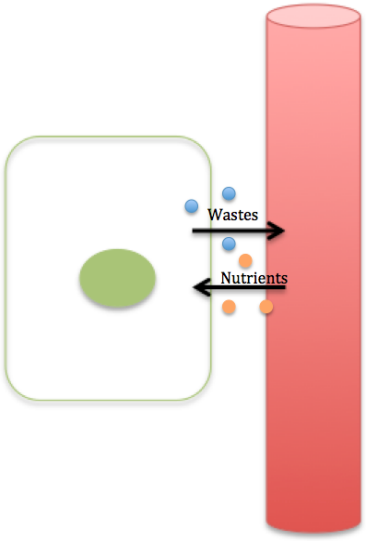

Fig. 3.1. Diagram of the interstitial space in which exchange occurs between the blood and cells.

The volume of the ICF, blood plasma, and interstitial fluid compartments in rats is assumed to be 33%, 4.5%, and 12% respectively (Caputo, 1989). Due to Tf binding, it is hypothesized Pu will initially be in the ECF and the value of V_C will be less than or equal to 16.5% of body weight. After 24 hours, cellular uptake and organ retention of Pu is anticipated. This should result in a V_D greater than 16.5% of body weight.

The young adult female S-D rats from which the Durbin data was collected were reported to have an approximate body weight of 250 g (Durbin 1972). Therefore, it is hypothesized V_C calculated using this data will be less than or equal to the ECF volume of 41.3 mL. V_D will be greater than 41.3 mL for rats sacrificed at the 24 hour time point.

The F344 rats examined in the LRRI study had a body weight of 157 ± 6 g for females and 235 ± 13 g for males (Weber et al. 2014). The weight range amongst all rats was 130 g to 450 g. The ECF volumes of 25.9 mL, 38.8 mL, 32.3 mL will be compared to the V_D values calculated for females, males, and experimental group averages (both male and female). A sensitivity analysis will be performed to account for the spread of body weights (see Appendix D). This involves the calculation of V_D using body weights plus and minus the standard deviations. These values will be used to determine if body weight variance influences V_D enough to change conclusions about physiological behavior.

Chapter 4: Data Analysis and Results

4.1 Plasma Concentration Time Profiles

Drawing a blood sample and administering an IV injection simultaneously is an impractical approach for determining C_0. It is a difficult process to perform on small animals such as rats and the results obtained are unlikely to represent uniform distribution within the central compartment (Schrag & Regal, 2013). For this reason it is necessary to find C_0 via extrapolation. The online curve fitting tool using Python source code ZunZun[1] was used to find the best-fit exponential curve for C_P versus time (Fig. 4.1). The best-fit curve to the Durbin data was a double exponential with an R^2 value of 0.998:

$$y = a * \exp(bx) + c * \exp(dx) \quad (4.1)$$

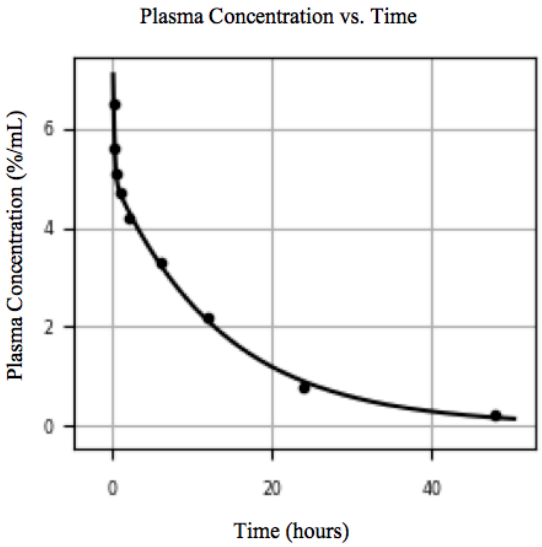

Fig. 4.1. Plasma concentration time profile of IV injected $^{239}Pu^{4+}$-citrate using Durbin data.

[1] zunzun.com
James R. Phillips
2548 Vera Cruz Drive
Birmingham, AL 35235 USA
James R. Phillips
2548 Vera Cruz Drive
Birmingham, AL 35235 USA

The coefficients of this nonlinear regression model are a = 5.01, b = -7.21, c = 3.07, and d = -5.65. C_0 was found by solving the equation for x = 0. The resulting C_0 was 8.08 %/mL.

The best-fit to the LRRI female data was an exponential with coefficients a = 1.73 and b = -5.56 with $R^2 = 0.922$ (Fig. 4.2). C_0 was calculated to be 1.73 %/mL.

$$y = a * exp(bx) \tag{4.2}$$

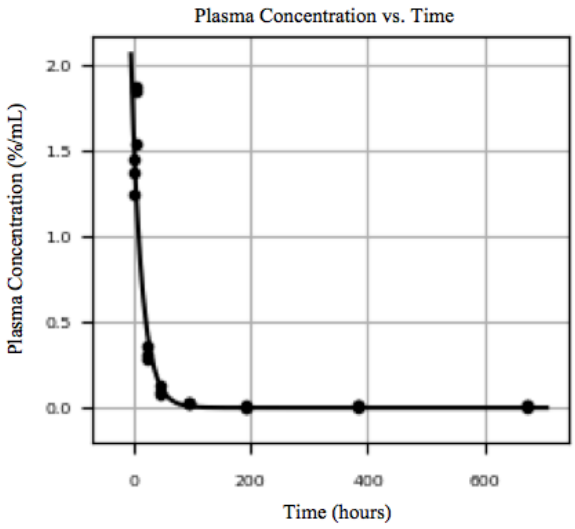

Fig. 4.2. Plasma concentration time profile of IV injected $^{239}Pu^{4+}$-citrate using LRRI female data.

The male rat data was best-fit with an exponential curve with coefficients a = 0.89 and b = -4.53 (Fig. 4.3). The R^2 value for this fit is 0.869. The resulting C_0 for male rats in the LRRI study was 0.89 %/mL.

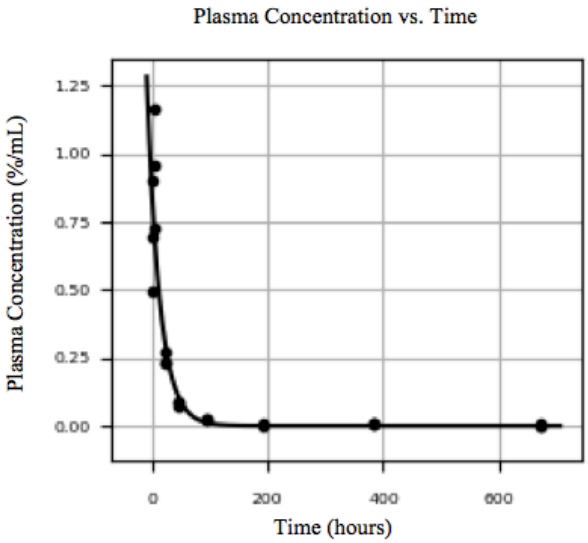

Fig. 4.3. Plasma concentration time profile of IV injected $^{239}Pu^{4+}$-citrate using LRRI male data.

The plasma concentration time profile for all LRRI rat data had a best-fit exponential with coefficients a = 1.31 and b = -5.18 (Fig. 4.4). This fit had and R^2 value of 0.799 and results in a C_0 of 1.31 %/mL.

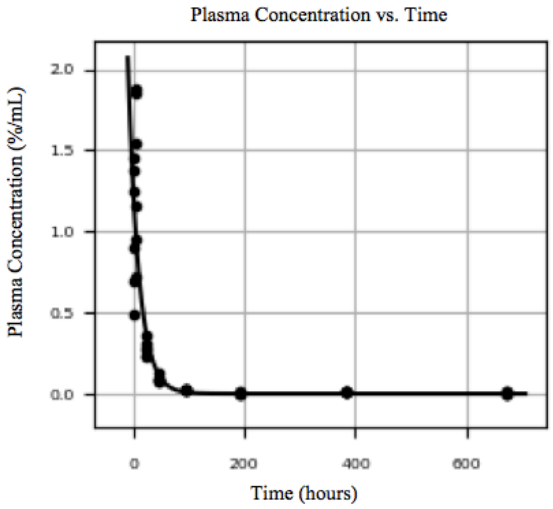

Fig. 4.4. Plasma concentration time profile of IV injected $^{239}Pu^{4+}$-citrate using LRRI rat data.

The plasma concentration time profiles provide key information about the distribution of Pu. It is interesting to note that while all LRRI data resulted in monoexponential equations, the

Durbin data was better described with a biexponential fit. The contrasting monophasic and biphasic distributions may be suggestive of physiological differences between S-D and F344 rats influencing ADME of Pu.

4.2 Volume of Distribution Time Profiles

The V_D time profiles illustrate increasing cellular uptake and tissue retention of Pu with time. A rise in V_D suggests more fluid volume is necessary to obtain measured C_P values. In drug design, V_D time profiles typically reach a plateau period of steady-state known as V_{SS}. V_{SS} represents the point at which the distribution phase has ended and movement of the compound between ECF and ICF is balanced (Mansoor 2019). Due to the complex biochemistry, relatively low concentrations, and physiological behavior of Pu, a steady-state is not seen in the V_D time profiles created for any of the data.

There is a biexponential relationship between V_D and time in the profile created using the Durbin data. The increase of V_D is consistent with the distribution of the compound as it is delivered from the blood to tissues where it is retained or recycled (Fig 4.5). V_{SS} is never reached suggesting the amount of material that has been taken into the cells is not returned to the blood at an equal rate.

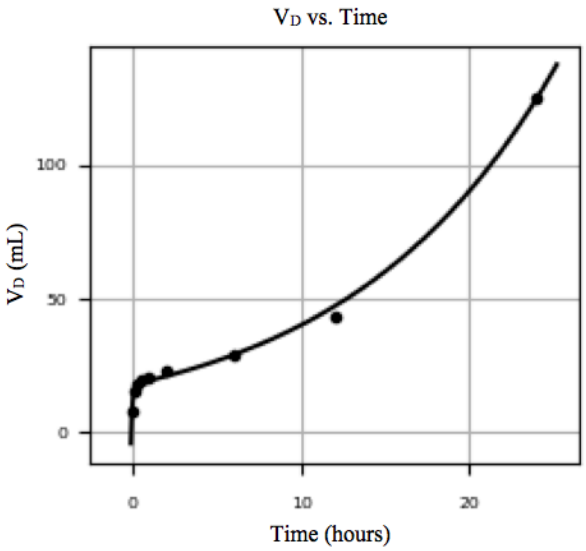

Fig. 4.5. V_D time profile for IV injected Pu using Durbin rat data.

Although there are some similarities between the Durbin and LRRI data, the V_D time profiles have some distinct features. The relationship between V_D and time for the female data is also described with a biexponential fit however there is a sharp increase of V_D for rats in the group sacrificed eight days after injection. The amount of activity recovered from the blood of animals in this necropsy group was relatively low compared to the trend. The resulting V_D time profiles suggests a large tissue deposition and subsequent release back to the blood occurred between four and 16 days after Pu was introduced to the system (Fig. 4.6).

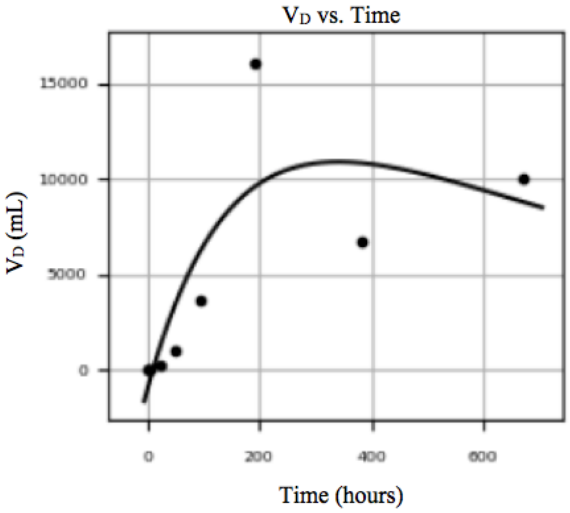

Fig. 4.6. V_D time profile for IV injected Pu using LRRI female rat data.

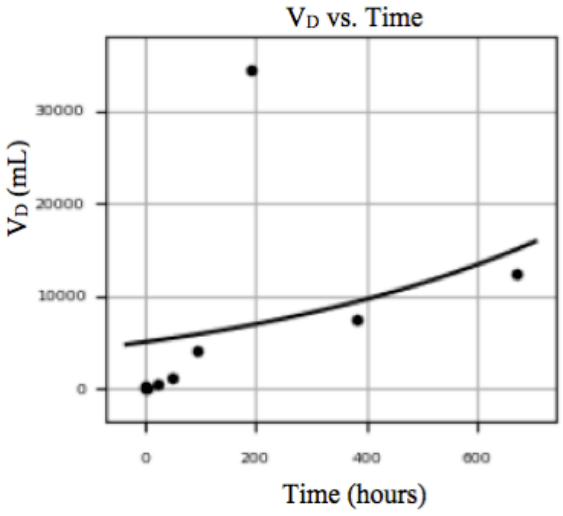

Fig. 4.7. V_D time profile for IV injected Pu using LRRI male rat data.

The V_D time profile for male rats was described with a monoexponential curve, however the spike on day eight resulted in a low closeness of fit (Fig. 4.7). A V_D time profile not including the data collected for the eighth day necropsy group may have a better fit and more closely resemble the curve generated using the Durbin data in Figure 4.5 (see Appendix B for LRRI V_D time profiles created without day 8 necropsy group data).

4.3 Identified Volume of Distribution

The values identified for V_C were compared to the ECF volume (Table 4.1). The V_C calculated using the Durbin data on young adult female S-D rats was 8.08 mL with a 95% confidence interval of [10.21, 15.73] (see Appendix C for confidence interval calculations). V_C is less than ECF volume with a confidence of 95% and is consistent with known behavior of Pu. Therefore, the null hypothesis is consistent and the alternate hypothesis is rejected.

Table 4.1: Identified values of V_C compared to ECF volume

Animal Data	V_C (mL)	ECF (mL)
Female S-D rats (Durbin)	8.08	41.25
Female F344 rats (LRRI)	57.93	25.09
Male F344 rats (LRRI)	111.98	38.78
Male & Female F344 rats (LRRI)	76.36	32.34

The V_C found using LRRI male rat data was significantly greater than ECF at 111.98 mL and a 95% confidence interval of [96.15, 133.51]. Calculations of V_C using female and combined male and female date from LRRI were also not consistent with known behavior of Pu. V_C was 57.93 with a confidence interval of [51.55, 66.23] for females rats. Given the high V_C in both males and females, their combined data also resulted in V_C not consistent with anticipated results. Therefore using the data provided by LRRI, the null hypothesis in this case was rejected and the alternate accepted.

Table 4.2: Identified values of V_D at time t = 24 hours compared to ECF volume

Animal Data	V_D at t = 24 hr (mL)	ECF (mL)
Female S-D rats (Durbin)	125.6	41.25
Female F344 rats (LRRI)	306.49	25.09
Male F344 rats (LRRI)	392.83	38.78
Male & Female F344 rats (LRRI)	349.66	32.34

Although the conclusions based on V_C values varied, the V_D at time t = 24 hours was greater than ECF in all cases and within a confidence level of 95% (Table 4.2). This result is consistent with the rapid delivery and retention of Pu in organ tissues. The Durbin data and all six rats from the 24 hour necropsy group in the LRRI studies supported this outcome.

Chapter 5: Conclusion

5.1 Discussion

The hypotheses tested in this research compared the calculated V_D at times t = 0 and t = 24 hours to the expected values based on known biological behavior of Pu-239. The null hypothesis using the Durbin data was consistent. The V_D at time t = 0 calculated for this data set was less than the determined volume of ECF. This is consistent with the idea that cellular uptake of Pu does not occur instantaneously at the time of injection. The V_D at time t = 24 hours was found to be greater than ECF volume. This was the anticipated result as tissue uptake and retention occurs once Pu has been distributed within the body.

The null hypothesis was rejected for the LRRI rat data. Although V_D at time t = 24 hours was greater than ECF as expected, the V_D at time t = 0 was also greater than ECF for both males and females. This result would suggest immediate delivery to cells and subsequent uptake of Pu at the time of IV administration. This is inconsistent with expected results and therefore the alternate hypothesis was accepted for this set of data. Although the null hypotheses for all F344 rats was rejected, the V_D values identified for female S-D rats are useful to move forward with the development of a PBPK model for Pu. The V_D time profiles generated in this research also still provide valuable information about the biological behavior of Pu in the body.

5.2 Future Work

The research in this work identified the V_C and V_D at time t = 24 hours for two sets of rat data. This study also generated V_D time profiles. Future work may include the replication of this study using data from a study in which measurements were collected over longer periods of time

after IV administration of Pu. This may result in a V_D time profile in which equilibrium is eventually achieved and V_{SS} can be determined. A longer time profile may also show a point at which Pu has reached an elimination phase under which a value known as V_{area} or V_β may be identified (Fig. 5.1).

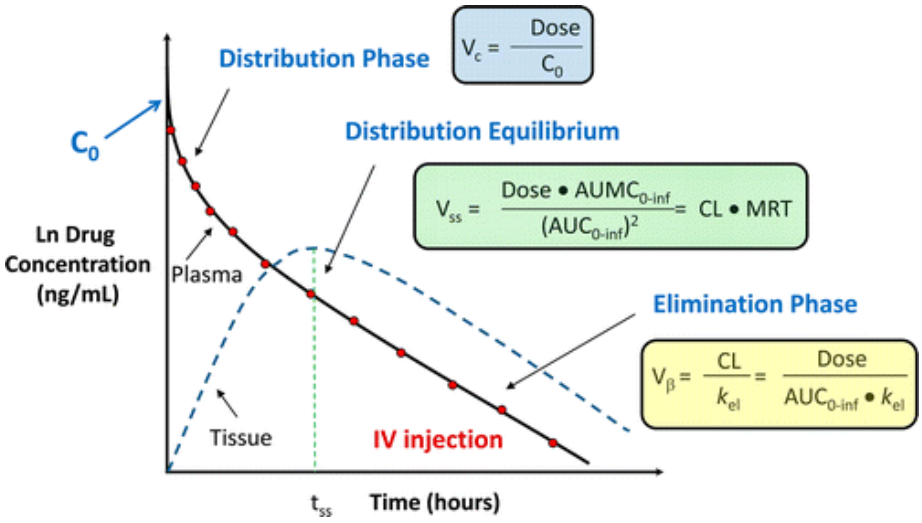

Fig. 5.1. Volume of distribution time profile demonstrating the values of V_D that can be found at different phases of ADME (Smith et al. 2015)

This work identified V_D, an important parameter for the development of a PBPK model. However the determination of additional parameters is still necessary. Future work may also include the identification of the elimination rate constant, k_{el}. As shown in Figure 5.1, this can be found using CL and V_β (Smith et al. 2015). This research has confirmed that the principle of V_D can be applied to Pu and is consistent with its known biological behavior in certain cases. With this information the effort to identify more physiological parameters of Pu in the endeavor to create a PBPK model may be continued.

References

Abbaspour, N., Hurrell, R., & Kelishadi, R. (2014) Review on iron and its importance for human health. *Journal of Research in Medical Sciences : The Official Journal of Isfahan University of Medical Sciences*, *19*(2), 164–174.

Baker, Heather M., Baker, Edward. (2012) A structural perspective on lactoferrin function. *Biochemistry and cell biology*. 90. 320-8. 10.1139/o11-071. Retrieved from https://www.researchgate.net/publication/221793826_A_structural_perspective_on_lactoferrin_function

Davis, P. J., Bosenburg, A., et al. (2011) Smith's Anesthesia for Infants and Children: Chapter 7 Pharmacology of Pediatric Anesthesia. 8th ed. 179-261. https://doi.org/10.1016/B978-0-323-06612-9.00007-9

Durbin, P.W. (2008) Actinides in Animals and Man. In: Morss L.R., Edelstein N.M., Fuger J. (eds) The Chemistry of the Actinide and Transactinide Elements. Springer, Dordrecht. Retrieved from https://link.springer.com/chapter/10.1007/1-4020-3598-5_31

Durbin, P.W., Horovitz, M.W., Close, E.R. (1972) Plutonium Deposition Kinetics in the Rat. *Health Physics*. Vol. 22, pp. 731-741. Retrieved from https://inldigitallibrary.inl.gov/PRR/89473.pdf

Gupta, C.P. (2014) Role of Iron (Fe) in Body. *Journal of Applied Chemistry* (IOSR-JAC)e-ISSN: 2278-5736.Volume 7, Issue 11 Ver. II, PP38-46. Retrieved from https://pdfs.semanticscholar.org/f242/cd23c65c0b77dd17859208792ea96ae2917d.pdf

Insel, P., Ross, D., McMahon, K., Bernstein, M. (2011) *Nutrition*. 4th ed. Jones & Bartlett Learning. Burlington, MA.

Jensen, M. P., Gorman-Lewis, D., et al. (2011) An iron-dependent and transferrin-mediated cellular uptake pathway for plutonium. *Nature Chemical Biology*, *7*(8), 560–565. http://doi.org/10.1038/nchembio.594

Jones, E. (2002) Process for producing ultra-pure plutonium-238. https://patents.google.com/patent/US6896716B1/en

Kohgo, Y., Ikuta, K., Ohtake, T., Torimoto, Y., & Kato, J. (2008) Body iron metabolism and pathophysiology of iron overload. *International journal of hematology*, *88*(1), 7–15. doi:10.1007/s12185-008-0120-5

Konzen K, Miller S, Brey R. (2015) Proposed Modification to the Plutonium Systemic Model. *Health Phys.* 109(4):307-318.

Kuepfer, L., Niederalt, C., et al. (2016) Applied Concepts in PBPK Modeling: How to Build a PBPK/PD Model. *CPT: pharmacometrics & systems pharmacology*, *5*(10), 516–531. doi:10.1002/psp4.12134

LANL. Periodic Table of Elements. https://periodic.lanl.gov/94.shtml

Lee, H.B., Blaufox, M.D. (1985) Blood volume in the rat. *Journal of Nuclear Medicine,* 26(1):72-6. Retrieved from https://www.ncbi.nlm.nih.gov/pubmed/3965655

Mansoor A, Mahabadi N. Volume of Distribution. (2019) In: StatPearls [Internet]. Treasure Island (FL): StatPearls Publishing. Retrieved from: https://www.ncbi.nlm.nih.gov/books/NBK545280/

Moss, W., Eckhardt, R. (1995) The Human Plutonium Injection Experiments. *Los Alamos Science*, 23:177-233. Retrieved from: https://fas.org/sgp/othergov/doe/lanl/pubs/00326640.pdf

Oakley S. Space Exploration: Improved planning and communication needed for plutonium-238 and radioisotope power systems production. http://large.stanford.edu/courses/2018/ph241/shi2/docs/gao-18-161t.pdf

Priest, N.D. (1990) The Distribution and Behavior of Heavy Metals in the Skeleton and Body: Studies with Bone-Seeking Radionuclides. In *Trace Metals and Fluoride in Bones and Teeth.* pp. 85-86. Boca Raton, FL: CRC Press.

Schrag, M., Regal, K. (2013) Pharmacokinetics and Toxicokinetics. *A Comprehensive Guide to Toxicology in Nonclinical Drug Development.* 2nd ed.

Schubert, J., Fried, J., Rosenthal, M., & Lindenbaum, A. (1961) Tissue Distribution of Monomeric and Polymeric Plutonium as Modified by a Chelating Agent. *Radiation Research, 15*(2), 220-226. DOI:10.2307/3571253

Seaborg GT, McMillan EM, Kennedy JW, Wahl AC. (1946) Radioactive element 94 from deuterons. Phys Rev 69:366-367 https://journals.aps.org/pr/pdf/10.1103/PhysRev.69.366.2

Smith, D.A., Beaumont, K., Maurer, T.S., and Di, L. (2008) Volume of Distribution in Drug Design. *Journal of Medicinal Chemistry 58* (15), 5691-5698. DOI: 10.1021/acs.jmedchem.5b00201

Smolin, L. A., & Grosvenor, M. B. (2010) *Nutrition: Science and applications*. 2nd ed. John Wiley & Sons, Inc. Hoboken, NJ.

Spruill, W.J., Wade, W.E., et al. (2014) Concepts in Clinical Pharmacokinetics: Chapter 2 Basic Pharmacokinetics. 6th ed. https://www.ashp.org/-/media/store-files/p3873-frontmatter.ashx

Steere, A. N., Byrne, S. L., Chasteen, N. D., & Mason, A. B. (2012) Kinetics of iron release from transferrin bound to the transferrin receptor at endosomal pH. *Biochimica et Biophysica Acta*, *1820*(3), 326–333. Retrieved from http://doi.org/10.1016/j.bbagen.2011.06.003

Taylor, D.M. (1973) Chemical and physical properties of plutonium. In Uranium, Plutonium, Transuranic elements. Eds: Hodge HC, Stannard JN, Hursch JB. Springer –Verlag, Heidelberh: 323-347.

Turgeon, Mary Louise. (2012) *Clinical Hematology: Theory and Procedures*. 5th ed. Wolters Kluwer: Lippincott Williams & Wilkins. Philadelphia, PA.

U.S. NRC. (2017) Background on Plutonium. https://www.nrc.gov/reading-rm/doc-collections/fact-sheets/plutonium.html

Wally, J., Halbrooks, P. J., Vonrhein, C., Rould, M. A., Everse, S. J., & Mason, A. B. (2006) The Journal of Biological Chemistry 281, 23934-23944. Retrieved from http://www.jbc.org/content/281/34/24934.full

Weber, W., Doyle-Eisele, M., Melo, D.R., Guilmette, R. (2014) Whole-body distribution of plutonium in rats for different routes of exposure. *International Journal of Radiation Biology.* 90(11): 1011–1018.

Whitney, E. N., & Rolfes, S. R. (2011) *Understanding Nutrition*. 12th ed. Cengage Learning. Boston, MA.

Appendix A

LRRI data used for the calculation of V_D

Table A.1: Data used for V_D calculations of LRRI rat data

Rat	Time of Necropsy (hr)	Urine	Feces	Total excretion	Blood
F1	1	0.00	1.30	1.30	14.75
F2	1	0.00	0.94	0.94	12.67
F3	1	1.81	0.14	1.94	13.97
F4	1	3.99	0.02	4.01	10.38
F5	1	5.79	0.04	5.84	13.45
F6	1	0.00	0.00	0.00	7.33
E1	4	0.54	0.04	0.57	15.77
E2	4	1.82	0.02	1.84	18.92
E3	4	2.30	0.06	2.36	19.10
E4	4	2.80	0.05	2.85	14.19
E5	4	0.59	0.06	0.65	17.28
E6	4	2.29	0.02	2.31	10.76
D1	24	2.53	2.06	4.59	3.67
D2	24	1.64	2.44	4.08	2.85
D3	24	2.01	2.26	4.27	3.14
D4	24	1.29	3.17	4.46	3.47
D5	24	1.22	1.61	2.83	4.09
D6	24	2.31	2.38	4.69	3.41
G1	48	2.07	4.00	6.07	0.85
G2	48	1.82	2.38	4.20	0.89
G3	48	4.57	2.84	7.41	1.26
G4	48	2.75	3.48	6.23	1.13
G5	48	1.85	4.40	6.25	1.35
G6	48	1.38	2.52	3.90	1.26
C1	96	8.75	5.00	13.75	0.27
C2	96	3.03	4.31	7.34	0.24
C3	96	6.09	4.06	10.15	0.24
C4	96	0.73	8.23	8.95	0.35

C5	96	2.10	8.05	10.16	0.32
C6	96	3.13	8.61	11.74	0.34
H1	192	2.68	9.31	11.98	0.11
H2	192	2.64	10.23	12.87	0.06
H3	192	2.66	18.25	20.91	0.03
H4	192	4.06	14.87	18.93	0.02
H5	192	2.92	14.24	17.16	0.00
H6	192	3.67	12.93	16.59	0.11
B1	384	3.96	19.78	23.74	0.08
B2	384	2.17	22.25	24.43	0.12
B3	384	3.90	15.31	19.21	0.17
B4	384	6.42	17.98	24.40	0.14
B5	384	4.86	22.53	27.39	0.16
B6	384	5.13	19.09	24.22	0.15
A1	672	5.14	27.59	32.73	0.18
A2	672	5.81	27.94	33.75	0.04
A3	672	4.40	28.05	32.45	0.10
A4	672	3.97	28.97	32.94	0.14
A5	672	3.40	29.99	33.38	0.06
A6	672	6.72	26.68	33.40	0.07

Appendix B

LRRI V_D time profiles without day 8 necropsy group

The V_D time profile generated using the LRRI male rat data excluding the day 8 necropsy group is best-fit with a double exponential curve. The R^2 value is 0.99 for this model. The R^2 for the model including the eighth day data shown in Figure 4.7 is 0.12. It is seen the omission of day 8 necropsy group data results in a closer fit model.

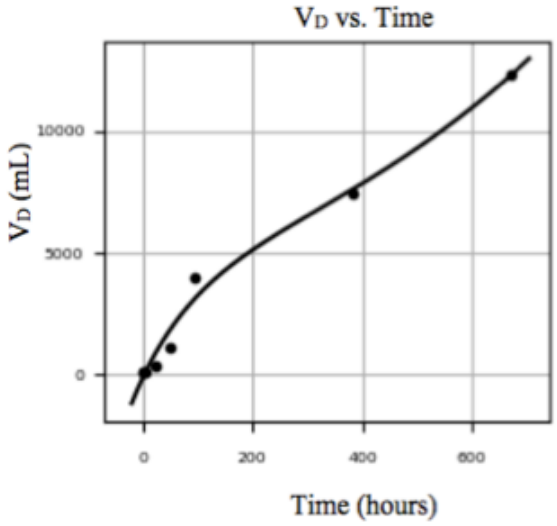

Fig. B.1. V_D time profile for LRRI male rat data excluding day 8 necropsy group.

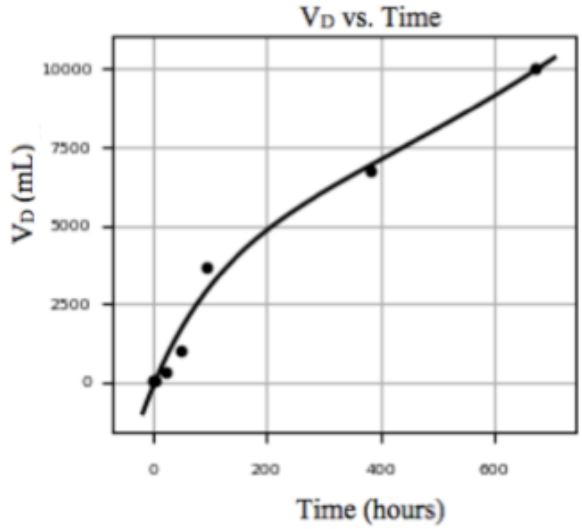

Fig. B.2. V_D time profile for LRRI female rat data excluding day 8 necropsy group.

The same result is true for the female rat data. Figure 4.6 is a biexponential best-fit with an R^2 of 0.71. The best-fit curve to the data excluding the eighth day necropsy group is also a biexponential however a better fit is shown with the R^2 value equal to 0.99.

Appendix C

95% Confidence Interval Calculations for V_D

The confidence intervals were determined for V_D using the 95% confidence intervals for the best-fit curve to the plasma concentration time profile using ZunZun. Each coefficient of the equation was assigned a 95% confidence interval. The equation of the line using the 95% confidence interval values and solving for x = 0 and x = 24 were the resulting confidence intervals for calculated C_P values. C_P values were then used in the calculation of V_D using equation 1.1.

The Durbin data was best-fit with a double exponential curve (Eq. 4.1). The 95% confidence intervals for coefficients a, b, c, and d were [4.75, 5.27], [-0.82, -0.63], [1.61, 4.53], and [-9.16, -2.14] respectively. This resulted is a 95% confidence interval of [10.21, 15.73] for V_C and [80.30, 140.90] for V_D at time t = 24 hours.

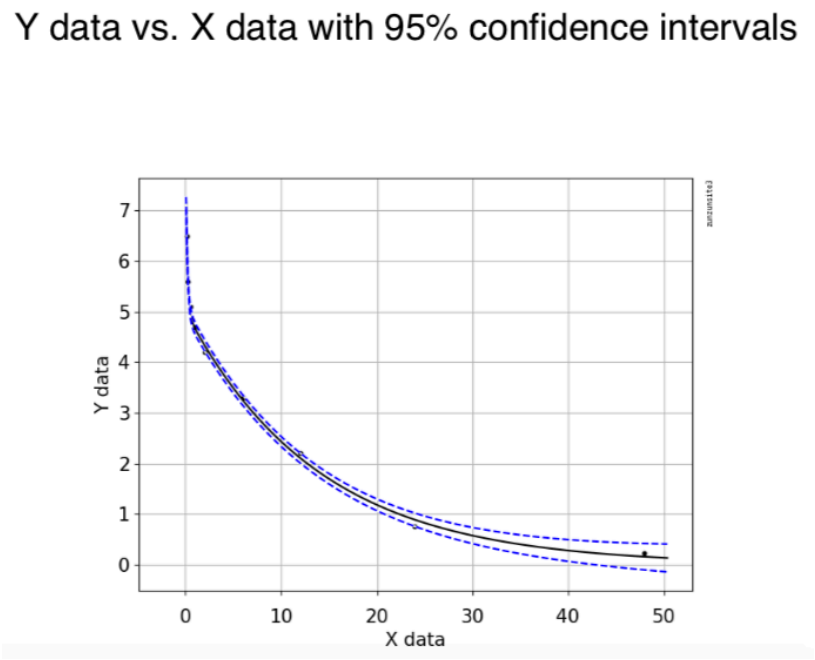

Fig. C.1. 95% confidence interval fit to plasma concentration versus time output from ZunZun for Durbin rat data.

The same method was used for male and female LRRI rat data. The plasma concentration time profiles for this dataset were best-fit with a monoexponential curve. The coefficients a and b for the male rats had a confidence interval of [0.75, 1.04] and [-0.07, -0.02] respectively. This resulted in a 95% confidence interval of [96.15, 133.51] for V_C and [167.80, 621.81] for V_D at time t = 24 hours.

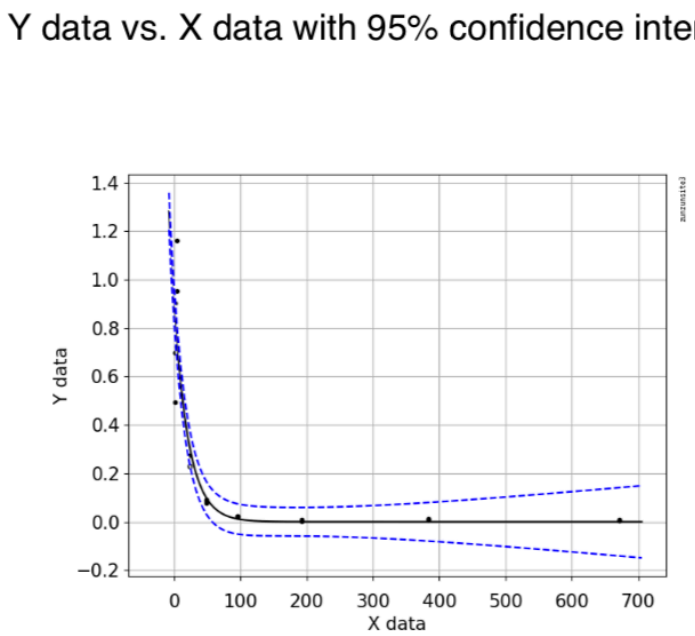

Fig. C.2. 95% confidence interval fit to plasma concentration versus time output from ZunZun for LRRI male rat data.

The 95% confidence interval for a and b of the monoexponential curve best-fit to the female LRRI data were [1.51, 1.94] and [-0.08, -0.04]. This resulted in a 95% confidence interval of [51.55, 66.23] for V_C and [115.91, 388.94] for V_D at time t = 24 hours.

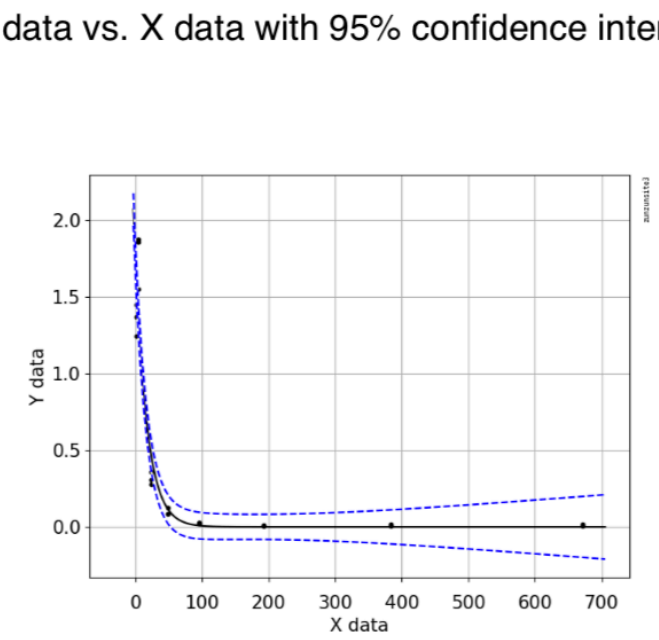

Fig. C.3. 95% confidence interval fit to plasma concentration versus time output from ZunZun for LRRI female rat data.

Appendix D

Sensitivity analysis to account for spread of body weights in LRRI rat data

The impact of the spread of BW provided in the LRRI data was tested with a sensitivity analysis. The standard deviations for male and female BW were used to calculate BV using equation 3.2 (Table D.1.). The C_P was then calculated by dividing the recovered % activity in blood by average BW ± standard deviation for male and female rats. C_P values were then used to solve for V_D using equation 1.1.

Table D.1: BV calculated for male and female rats using average and ± standard deviation BW

Average			
Female BW (g)	Female BV (ml)	Male BW (g)	Male BV (ml)
157	10.19	235	14.87
- STD			
Female BW (g)	Female BV (ml)	Male BW (g)	Male BV (ml)
151	9.83	222	14.09
+ STD			
Female BW (g)	Female BV (ml)	Male BW (g)	Male BV (ml)
163	10.55	248	15.65

The resulting V_D values were then compared to those calculated using average body weights (Table D.2). Although V_D values varied, the change was not great enough to draw conclusions different from those made about V_D values calculated using average body weights.

Table D.2: V_D calculated for LRRI rats using average and ± standard deviation BW

Rat	**Time of Necropsy (hr)**	**V_D (ml) (Avg BW)**	**V_D (ml) (-STD)**	**V_D (ml) (+STD)**
F1	1	68.18	65.77	70.58
F2	1	79.69	76.88	82.51
F3	1	71.51	68.99	74.04
F4	1	137.54	130.33	144.76

F5	1	104.07	98.62	109.53
F6	1	202.75	192.12	213.39
E1	4	64.26	61.99	66.53
E2	4	52.88	51.01	54.75
E3	4	52.10	50.26	53.94
E4	4	101.83	96.49	107.17
E5	4	85.49	81.01	89.98
E6	4	135.04	127.96	142.12
D1	24	264.71	255.36	274.06
D2	24	343.57	331.44	355.71
D3	24	311.18	300.18	322.17
D4	24	409.18	387.71	430.64
D5	24	353.45	334.91	371.99
D6	24	415.87	394.05	437.68
G1	48	1131.42	1091.44	1171.39
G2	48	1099.33	1060.49	1138.16
G3	48	746.43	720.06	772.80
G4	48	1229.62	1165.12	1294.12
G5	48	1035.73	981.40	1090.06
G6	48	1134.99	1075.45	1194.52
C1	96	3231.32	3117.16	3345.47
C2	96	3967.29	3827.13	4107.45
C3	96	3814.92	3680.15	3949.70
C4	96	3846.30	3644.55	4048.06
C5	96	4174.94	3955.94	4393.93
C6	96	3894.48	3690.20	4098.77
H1	192	8153.57	7865.52	8441.63
H2	192	13873.37	13383.24	14363.50
H3	192	25996.99	25078.55	26915.43
H4	192	57408.11	54396.79	60419.43
H5	192	0	0	0
H6	192	11483.91	10881.52	12086.29
B1	384	9251.43	8924.59	9578.27
B2	384	6210.56	5991.15	6429.97

B3	384	4871.36	4699.26	5043.46
B4	384	8087.78	7663.54	8512.02
B5	384	6706.09	6354.33	7057.86
B6	384	7562.94	7166.23	7959.65
A1	672	3829.39	3694.10	3964.68
A2	672	19287.34	18605.94	19968.74
A3	672	6883.35	6640.17	7126.53
A4	672	7278.27	6896.49	7660.05
A5	672	15478.04	14666.15	16289.94
A6	672	14353.86	13600.93	15106.79